Materials and Design 187 (2020) 108404

Contents lists available at ScienceDirect

Materials and Design

journal homepage: www.elsevier.com/locate/matdes

Preparation of robust aramid composite papers exhibiting water resistance by partial dissolution/regeneration welding

Ke Xu [a,b], Yanghao Ou [a,b], Yinghui Li [a,b], Lingfeng Su [a,b], Meiyan Lin [a,b], Yang Li [a,b], Jiedong Cui [a,b], Detao Liu [a,b,*]

[a] State Key Laboratory of Pulp and Paper Engineering, South China University of Technology, Guangzhou 510640, China
[b] Guangdong Engineering Research Center for Green Fine Chemicals, South China University of Technology, Guangzhou 510640, China

HIGHLIGHTS

- The para-aramid/meta-aramid composite papers, exhibiting amazing mechanical strengths, were obtained.
- The performance of the para-aramid/meta-aramid composite paper was improved by adding *N*,*N*-dimethylacetamide/LiCl solution.
- The moisture absorption of aramid composite paper decreased from approximately 143% for the original paper to approximately 54%.

GRAPHICAL ABSTRACT

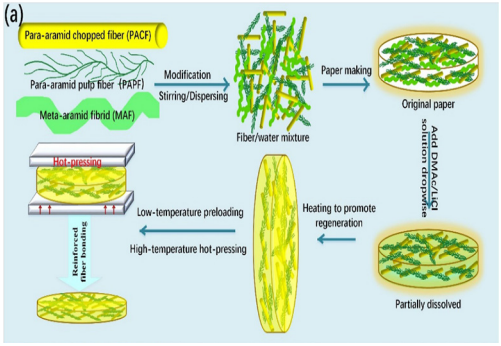

ARTICLE INFO

Article history:
Received 30 October 2019
Received in revised form 2 December 2019
Accepted 2 December 2019
Available online 06 December 2019

Keywords:
Aramid composites
Partial dissolution
Regeneration welding
Mechanical properties
Reinforcement

ABSTRACT

Aramid fibers exhibit impressive mechanical properties, electrical insulation properties, and chemical stability. However, physical properties of the aramid paper are poor because of the chemical inertness and smooth surface of aramid fibers. This study reports a simple and efficient method for substantially improving the performance of the para-aramid/meta-aramid composite paper by introducing the *N*,*N*-dimethylacetamide (DMAc)/LiCl solution to induce partial dissolution or by adding the DMAc/LiCl/para-aramid solution to induce regeneration. Experimental results state that the tensile strength, specific strength, folding resistance, and interlayer bonding strength of the aramid paper are increased by 2.17, 2.13, 34.7, and 9.39 times, respectively, because of the dense and compact structure of the paper. Furthermore, the water resistance of the paper was also considerably improved. After immersing the paper samples in water for 24 h, their moisture absorption rate decreased to approximately 54% from approximately 143% for the original paper. Results indicate that partial dissolution/regeneration welding is a viable method for the efficient reinforcement of the aramid composite paper, providing additional possibilities for manufacturing the high-performance aramid paper-based materials.

1. Introduction

Aramid fibers exhibit various surprising properties, such as ultrahigh specific strength and specific modulus, satisfactory high-temperature resistance and insulation, good chemical stability, and good flame

* Corresponding author.
E-mail address: dtliu@scut.edu.cn (D. Liu).

https://doi.org/10.1016/j.matdes.2019.108404

retardancy, thereby attracting significant research attention [1–5]. The aramid fiber composite materials have also been extensively used in military and civilian applications [6–10]. They are mainly classified into para- and meta-aramid fibers according to the position of the groups on their molecular chain; both these fibers exhibit excellent properties [11]. Aramid paper materials are generally manufactured from the aramid chopped fibers or aramid pulp fibers via papermaking wet mixing. They inherit several excellent properties of the aramid fibers and exhibit good reworkability and redesignability [12], thereby making it extensively applicable in high-tech fields such as rail transit [13], electronics [14–16], aerospace [17], and defense; furthermore, it plays an important role in modern industries.

The strength of the aramid paper is mainly derived from the random physical bridging between fibers to produce hydrogen bonding and from the rigidity of the fibers themselves [18]. However, unlike plant fibers, the aramid fibers exhibit a smooth and extremely chemically inert surface [19], resulting in a lack of sufficient hydrogen bonding between the aramid fibers. In addition, the poor hydrophilicity of the fibers results in their poor dispersion in aqueous media, resulting in the poor formation of the finished paper. Therefore, it is difficult to often achieve aramid paper with good mechanical properties without reinforcement, limiting the development and application of the aramid paper-based materials. Recently, researchers have extensively pursued solutions to the aforementioned problems. Chemical etching [20], coupling-agent modification [21,22], surface coating [23–26], plasma modification [27,28], high-energy radiation modification [29,30], and fluorination modification [31] can improve the surface activity of the aramid fibers to some extent. Enhanced surface activity promotes the dispersion of aramid fibers in water and formation of hydrogen bonds between fibers. Regardless, it is difficult to use these modification methods to qualitatively affect the mechanical strength of the aramid paper. Improving the mechanical properties of aramid paper remains an interesting but urgent problem.

In our previous researches [32,33], we observed that the cellulose fibers can be separated into nanofibers when ionic liquids and hot-pressing treatment are applied to the surface of the filter paper. With an increase in the hot-pressing time, nanofibers are observed to gradually dissolve and fill the gaps between fibers. The fibers that are not separated into filaments under pressure are welded with each other and hydrogen bonding force among the cellulose macromolecules is considerably enhanced, resulting in the transformation of the original paper into a dense and nonporous high-mechanical-strength transparent paper. The *N*,*N*-Dimethylacetamide (DMAc)/LiCl solution is a highly efficient solvent that can effectively dissolve several polymers, including cellulose [34,35] and PBI [36]. The meta-aramid fibers can also be completely dissolved in the DMAc/LiCl solution [37]. The technology for preparing meta-aramid nanofibers via the DMAc/LiCl/meta-aramid solution spinning has been developed [38–40], reflecting that the meta-aramid nanofibers exhibit good regeneration performance in the solution. Furthermore, the dissolution mechanism of the meta-aramid in the DMAc/LiCl solution and image of the solution are depicted in Fig. 1c and b, respectively.

Herein, we report simple and efficient method for substantially improving the properties of the para-aramid/meta-aramid composite paper by introducing the DMAc/LiCl solution to partially dissolve the original paper (Fig. 1a) or by adding the DMAc/LiCl/meta-aramid solution to regenerately strengthen the paper (Fig. 2). Experimental results show that the tensile strength, specific strength, folding resistance, and ILSS of the paper increased by 2.17, 2.13, 34.7, and 9.39 times, respectively, than those of the paper not treated with DMAc/LiCl. The water resistance of the paper was also considerably improved; after the paper was immersed in water for 24 h, its moisture absorption decreased from approximately 143% for the original paper to approximately 54%.

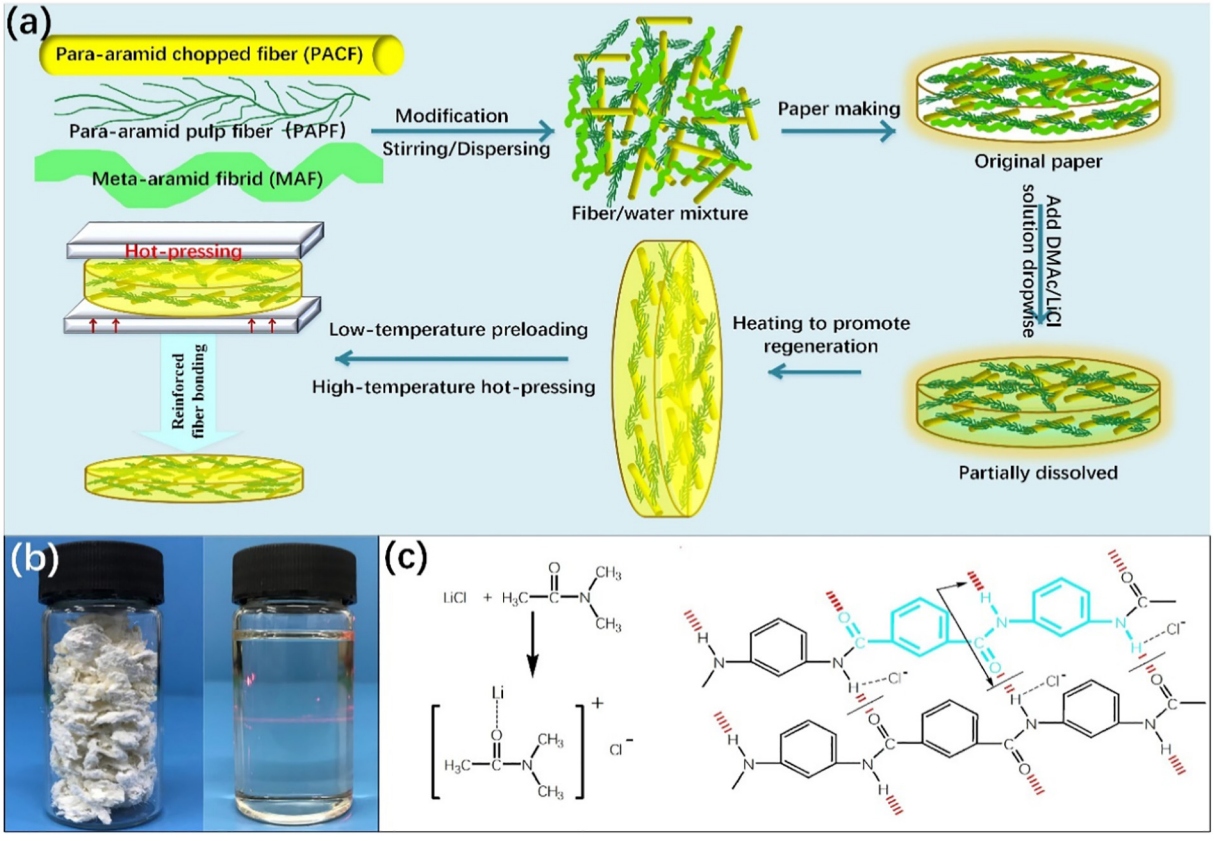

Fig. 1. (a) The simple manufacturing process of the partially-dissolved paper (PDP). (b) Digital photos of the meta-aramid fibrids (MAFs) and the DMAc/LiCl/meta-aramid solution. (c) Dissolution mechanism of meta-aramid in the DMAc/LiCl solution.

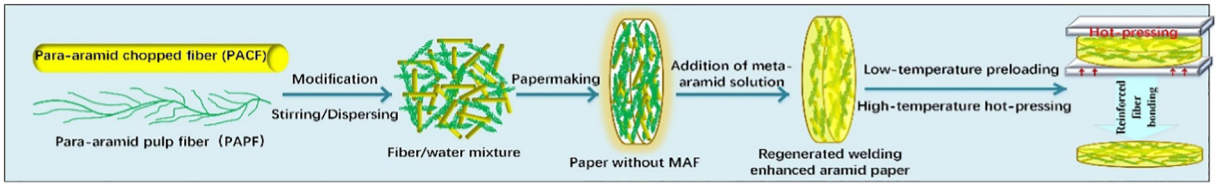

Fig. 2. The simple manufacturing process of the regeneratively welding-paper (RWP).

2. Materials and methods

2.1. Materials

The para-aramid chopped fibers (PACFs) and para-aramid pulp fibers (PAPFs) with an average length 5–6 mm were purchased from DuPont. Meta-aramid fibrids (MAFs) were provided by the Hyosung Group, Korea. All the polyoxyethylenes (PEOs) ($3{,}000{,}000 \le M_w \le 4{,}000{,}000$) were supplied by Shanghai Maclean Biochemical Technology Co. The coupling agent, *N*-(2-aminoethyl)-3-aminopropyltrimethoxysilane (KH-792), was provided by Jiangsu Chenguang Coupling Agent Co. DMAc and lithium chloride (LiCl) was obtained from Aladdin-Reagent Co., Ltd. (Shanghai, China). Acetone was supplied by Tianjin Fuyu Fine Chemical Co., Ltd. All the reagents were used as received without further purification.

2.2. Preparation of the original aramid paper

To produce the para-aramid/meta-aramid composite paper with a basis weight of 40 g/m^2, the PACFs, PAPFs, and MAFs were mixed with a handsheet former (MESSMER 255) in a mass ratio of 4:2:4; this paper was used for strengthening by the partial dissolution–regeneration. In addition, the paper without MAFs and with a basis weight of 24 g/m^2 was manufactured with the same amount of PACFs and PAPFs used in the aforementioned method; this paper was used for all meta-aramid solution regeneratively welding enhancement. Furthermore, the fibers were washed and modified according to our previously reported methods [22] before paper making. The fibers were separated into single fibers in water using a pulp disintegrator (L&W 991509, Sweden). The number of rotations was 3.0×10^4 and rotation speed was 6×10^3 rpm. When the separation was performed, 0.5 wt% PEO was added as a dispersant to the fiber suspension. Finally, all the fiber suspensions were poured into the handsheet former and dehydrated into a paper simultaneously.

2.3. Preparation of the DMAc/LiCl/meta-aramid solution

Anhydrous LiCl (8 g) was added to DMAc (92 g) and stirred at room temperature until LiCl was completely dissolved to obtain a DMAc/LiCl solution. Dry MAFs (5 g) were added to the DMAc/LiCl solution and stirred at 80 °C for 3 h to obtain a DMAc/LiCl/meta-aramid solution; the stirring speed was 1500–2500 rpm.

2.4. Preparation of the high-performance aramid composite paper

The partially dissolved paper (PDP) was prepared by a simple process (Fig. 1a). First, the DMAc/LiCl solution was added dropwise to the paper until the entire paper structure was filled with the solution. The paper was further placed in the air at room temperature and MAFs in the paper were gradually dissolved. After the MAFs were completely dissolved, the paper was heated in a blast dryer (Shanghai Jinghong Experimental Equipment Co., Ltd.) to evaporate the DMAc so that the dissolved MAFs begin to regenerate. When the regeneration was completed, the paper was pre-pressed using a flat vulcanizer for 5 min; the pre-pressing temperature was 150 °C, and pressure was 10 MPa. Subsequently, a large amount of water was used to wash the paper for eliminating the residual DMAc/LiCl. Finally, PDP was obtained by hot-pressing for 5 min under temperature and pressure conditions of 220 °C and 10 MPa, respectively. The method for all meta-aramid solution regeneratively welding enhancement is shown in Fig. 2. Furthermore, the DMAc/LiCl/meta-aramid solution was added dropwise to the paper without MAFs. Importantly, the solution was evenly distributed in the paper structure. The amount of added solution was controlled to increase the basis weight of the paper to 40 g/m^2 when the solution was regenerated in the paper so that the meta-aramid content in the paper was 40%. Furthermore, the regeneratively welding-paper (RWP) was obtained by a pre- and hot-pressing treatment in accordance with the foregoing method.

2.5. Characterization

The structure of the aramid composite paper was studied using scanning electron microscopy (SEM). A JEM-100CXII scanning electron microscope operated at an accelerating voltage of 10 kV was used. Prior to the examination, the surface of the specimen was coated with a thin layer (20 nm) of gold. The tensile strength of the samples was measured using a universal tensile tester (Instron 5565, Instron Instruments Inc., USA) with a stretching velocity of 5 mm/min. To prevent the sample from slipping during the test, we wrapped two ends of the sample with filter paper, placed them into the fixture together, and tightened the screws as much as possible. The test sample size was 20 × 10 mm. Furthermore, the thickness was determined using a thickness tester (L&W, Sweden). The ILSS of the samples was measured using an internal bond tester (TMI model 80–01). Next, the folding resistance test of the paper was conducted using a double-chuck folding resistance tester (FRANK-PTI model S1 3505.0000). A thermogravimetric analyzer (TA Instruments model Q500, USA) was used to analyze the thermal properties of the PACFs, MAFs, and reinforced paper. The test temperature range was 20 °C–700 °C, and the heating rate was 10 °C/min with an air purge at a flow rate of 20 mL/min. The quantity of each sample was controlled between 4 and 8 mg during the test. Further, the X-ray diffraction (XRD) patterns of the MAFs before dissolution and of the regenerated meta-aramid were recorded using an X-ray diffractometer (D8 ADVANCE, Bruker Inc., Germany) equipped with an area detector and Cu–Kα radiation source ($\lambda = 0.154$ nm) operating at voltage of 40 kV and current of 40 mA. The scanning range of 2θ ranged from 5° to 65° at room temperature. The FT–IR spectra were recorded in a scanning range from 400 to 4000 cm^{-1} on a Vertex 70 (Bruker, Germany) spectrometer equipped with an attenuated total reflectance apparatus.

3. Results and discussion

3.1. Reinforcement process and principle

The DMAc/LiCl solution is an excellent solvent for MAFs; the dissolution mechanism is shown in Fig. 1c. The $(DMAcLi)^+$ macrocations were formed in the DMAc/LiCl solution system, which changed the charge distribution between the Li and Cl atoms. The Cl atoms carry a considerable negative charge; therefore, its ability to attack the H atom in the amide group of the meta-aramid molecular chain was considerably enhanced. Hydrogen bonds were formed between the Cl and H atoms, destroying the mesh of the aramid crystal region. Finally, the aramid

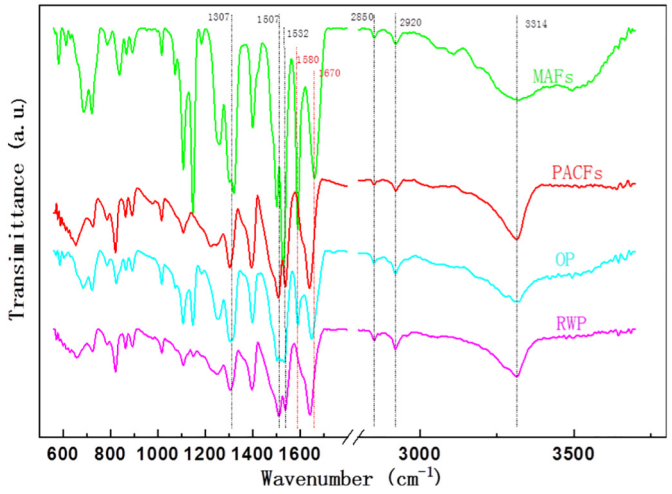

Fig. 3. The FT–IR spectra of the meta-aramid fibrids (MAFs), para-aramid chopped fibers (PACFs), the original paper (OP), and the regeneratively welding-paper (RWP).

macromolecular chain was dissociated and dissolved. The MAFs used to prepare the meta-aramid solution were agglomerated into white lumps before dissolution (Fig. 1b), and the resulting meta-aramid solution was clear and transparent (Fig. 1b). When the aramid paper was strengthened using partial dissolution–regeneration. (Fig. 1a), the original MAFs in the paper were completely dissolved by the DMAc/LiCl solution and were gradually dispersed in the paper structures. When the paper was reinforced with all meta-aramid solution regeneratively welding enhancement (Fig. 2), we directly added the DMAc/LiCl/meta-aramid solution to the paper without the meta-aramid pulp fiber; the aramid solution effectively filled the pore structure of the paper. When the paper was further heated, the hydrogen bonds between the $(DMAcLi)^+$ macrocations and the aramid molecular chains were destroyed.

The evaporation of the DMAc solution resulted in the reformation of the aramid crystalline zone. At this time, the regenerated meta-aramid coated the original PACFs and PAPFs in the paper structure to form a composite structure similar to that of the "steel-reinforced concrete." The hydrogen bond between the MAFs and para-aramid fibers was stronger than that in original paper (OP); in addition, the structure of paper was compact, thereby substantially improving the mechanical properties of the paper.

3.2. FT–IR analysis

We collected the FT–IR spectra of the MAFs, PACFs, OP, and RWP to study the hydrogen bonding between the fibers in the paper structure; the typical spectra are shown in Fig. 3a. Overall, the peak shapes and peak intensities of the OP are similar to those of the MAFs, whereas those of the RWP are similar to those of the PACFs. The absorption peak at 3314 cm^{-1} is assigned to the stretching vibration of the N—H bonds. The stretching vibration peak at 2920 and 2850 cm^{-1} originated from the —CH_2 and —CH_3 groups, respectively. The peaks at 1532 and 2850 cm^{-1} are attributed to the N—H deformation and C—N stretching coupled modes, respectively. The peak at 1507 cm^{-1} is caused by the stretching vibration of the C═C skeleton on a benzene ring, whereas that at 1307 cm^{-1} is assigned as amide band III (C—N bond stretching vibration, N—H in-plane bending vibration, and C—C bond stretching vibration) [41]. A comparison of the analysis results for the MAFs and the PACFs suggests that the infrared absorption strength of the MAFs at 4000–3300 and 1200–1600 cm^{-1} is greater than that of the PACFs; thus, the peak area of the MAFs is greater than that of the PACFs. Therefore, the degree of change in the dipole moment of the groups in the two main absorption wavenumber regions of the MAFs is greater than that of the groups in the two main absorption wavenumber regions of the PACFs, indicating that the groups of the MAFs are weakly restricted, possibly because the MAFs are less crystalline than the PACFs [42]. The FT-IR spectra of the OP and MAFs show two peaks at 1580 and 1670 cm^{-1}, representing the contractive vibration of the amide C═O bond (amide I band) to hydrogen and the contractive vibration of the aromatic C═O bond without any bonding, respectively. However, the spectra of the PACFs and RWP denote only a single peak with a considerable absorption intensity at 1640 cm^{-1} in this region; furthermore, the stretching vibration peak of the free aromatic C═O bonds disappeared because of the reduction of the carbonyl free radicals and increase in hydrogen bonding between the PACFs and the RWP [43]. In addition, the peak at 1532 cm^{-1} in the spectrum of the RWP was stronger than that in the spectrum of the OP, indicating that the hydrogen bonding in the RWP was enhanced [44]. More hydrogen bonding in the paper will

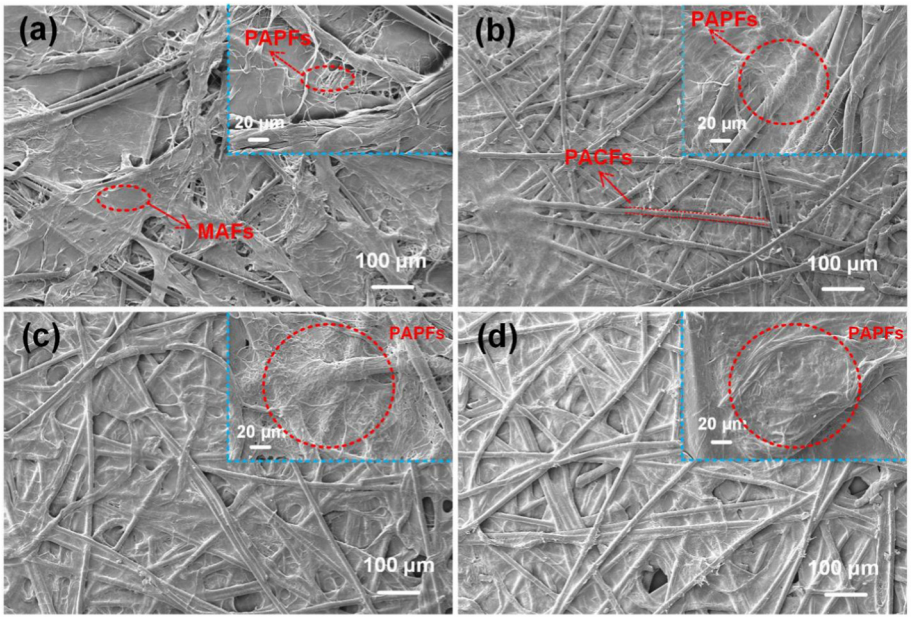

Fig. 4. The SEM images of the aramid paper surface: (a) original paper (OP); (b) hot-pressed paper (HP); (c) partially-dissolved paper (PDP); and (d) regeneratively welding-paper (RWP).

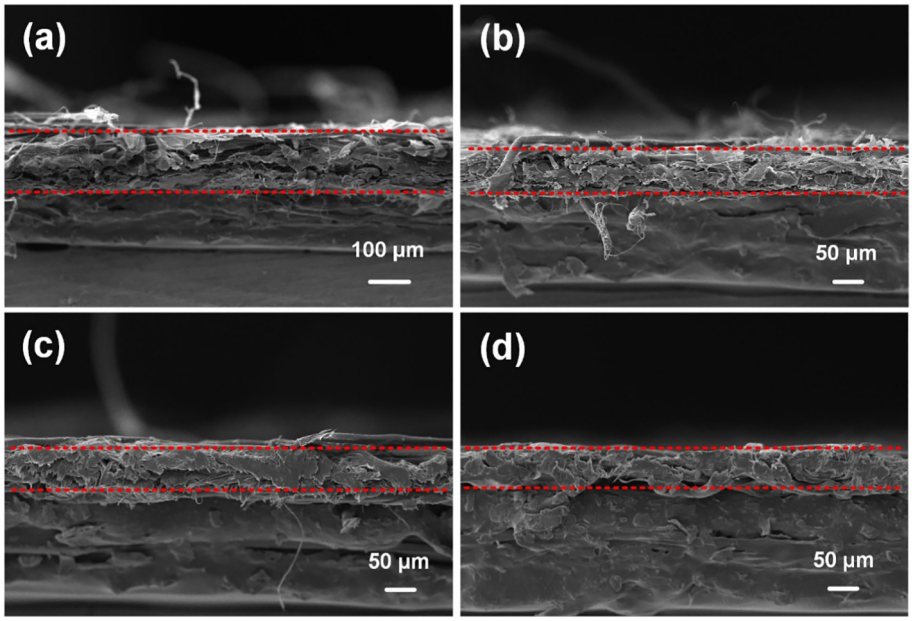

Fig. 5. The SEM micrographs of the fracture surface: (a) original paper (OP); (b) hot-pressed paper (HP); (c) partially-dissolved paper (PDP); and (d) regeneratively welding-paper (RWP).

undoubtedly lead to an improvement in mechanical strength, consistent with the results of the mechanical property tests.

3.3. Paper morphology analysis

To clearly observe the fiber combination in the paper, we characterized the morphology of the paper using SEM. The surface morphology of the OP is shown in Fig. 4a. The PAPFs are microfilaments with fine fibers and small specific surface area; the MAFs are flat and film-like with a large specific surface area, and the PACFs are rod-like with high rigidity. The three fiber types are connected only through a simple and loose physical overlap. Numerous microholes exist in the paper structure, and substantial portions of the PACFs and PAPFs are exposed on the surface of the paper. After hot-pressing at 10 MPa and 220 °C, the MAFs were plastically deformed and bonded closely with the PACFs and PAPFs; some of them were still exposed on the surface of the paper structure but they are less than the OP (Fig. 4b). The morphology of PDP is shown in Fig. 4c; the MAFs were completely dissolved, and their original morphology disappeared, resulting in the presence of a few pores in the paper. From the enlarged figure in the upper right corner, it can be seen that PACFs and PAPFs have been coated by the regenerated interposition aramid to some extent. The surface morphology of RWP is shown in Fig. 4d. In this case, the regenerated meta-aramid was completely filled with the paper structure. Upon comparing PACFs and PAPFs in the PDP, those in the RWP were more closely wrapped by the regenerated meta-aramid; in addition, the regenerated meta-aramid was more evenly distributed in the RWP than that in the PDP. All these factors are conducive to the formation of hydrogen bonds between the regenerated meta-aramid and the fibers in the OP. As shown in Fig. 5, the thickness of the OP was approximately 120 ± 15 μm, and the fibers in the paper were considerably loosely bonded (Fig. 5a). The thickness of the hot-pressed aramid paper (HP) was reduced to approximately 80 ± 10 μm; however, the paper structure was still insufficiently compact (Fig. 5b). The thicknesses of the PDP (Fig. 5c) and RWP (Fig. 5d) were approximately 75 ± 10 and 70 ± 10 μm, respectively. The fiber combination of the PDP and RWP was already considerably tight, which was undoubtedly beneficial for the mechanical strength of the pap.

3.4. Performance of the aramid paper composites

The tensile strength of the paper is presented in Fig. 6a and e. The average tensile strengths of the OP and HP were 6.75 and 24.1 MPa, respectively, and average tensile strengths of the PDP and RWP were 72.1 and 76.6 MPa, respectively. When compared with the average tensile strengths of the OP and HP, average tensile strength of the RWP increased substantially by 10.4 and 2.17 times, respectively (Fig. 7b).

Interestingly, the water resistance of the paper was considerably improved after completing the partial dissolution–regeneration and all meta-aramid solution regeneratively welding enhancement. After the HP was soaked in water for 24 h, its water absorption rate was observed to be as high as 142%. On the contrary, the water absorption rates of the PDP and RWP after 24 h of soaking were only approximately 54% (Fig. 6b). Moisture was eliminated from the surface of the samples using a filter sheet, and the samples were quickly subjected to testing with respect to their wet tensile strength. Results denote that the tensile strength of HP was considerably reduced by 73.7% after the sample was soaked in water, whereas the wet tensile strength of the PDP and the RWP remained approximately 40 MPa, exhibiting a loss of only 46.51% (Fig. 6c). At this time, the wet tensile strength of the RWP was 6.47 times greater than that of the HP. This difference is attributed to the fact that the paper structure of the PDP and the RWP is more compact than that of the HP and to the presence of fewer holes in the PDP and RWP, which makes water penetration into the paper difficult, diminishing the effect on hydrogen bonding in the paper structure.

The test results of the papers' folding resistance are shown in Fig. 7a. The average folding resistances of the OP and the HP were 4.5 and 20.5 times, whereas those of the PDP and full aramid solution regenerated composite paper reached an astonishing 550 and 732 times, respectively. The average folding resistance of the RWP was 161.7 and 34.7 times greater than those of the OP and the HP aramid composite paper, respectively (Fig. 7b). Notably, the better folding resistance of the two reinforced papers indicates that they exhibit good flexibility; the papers can be randomly folded into any shape (Fig. 7c). On the contrary, the use of a high-performance resin to augment the aramid paper tends to result in a substantial reduction in paper flexibility, which is extremely detrimental to the subsequent processing of the aramid paper [45]. The test results of ILSS are similar to those of the folding resistance (Fig. 7a). The average ILSS of the OP and the HP were as low as 70.2 and

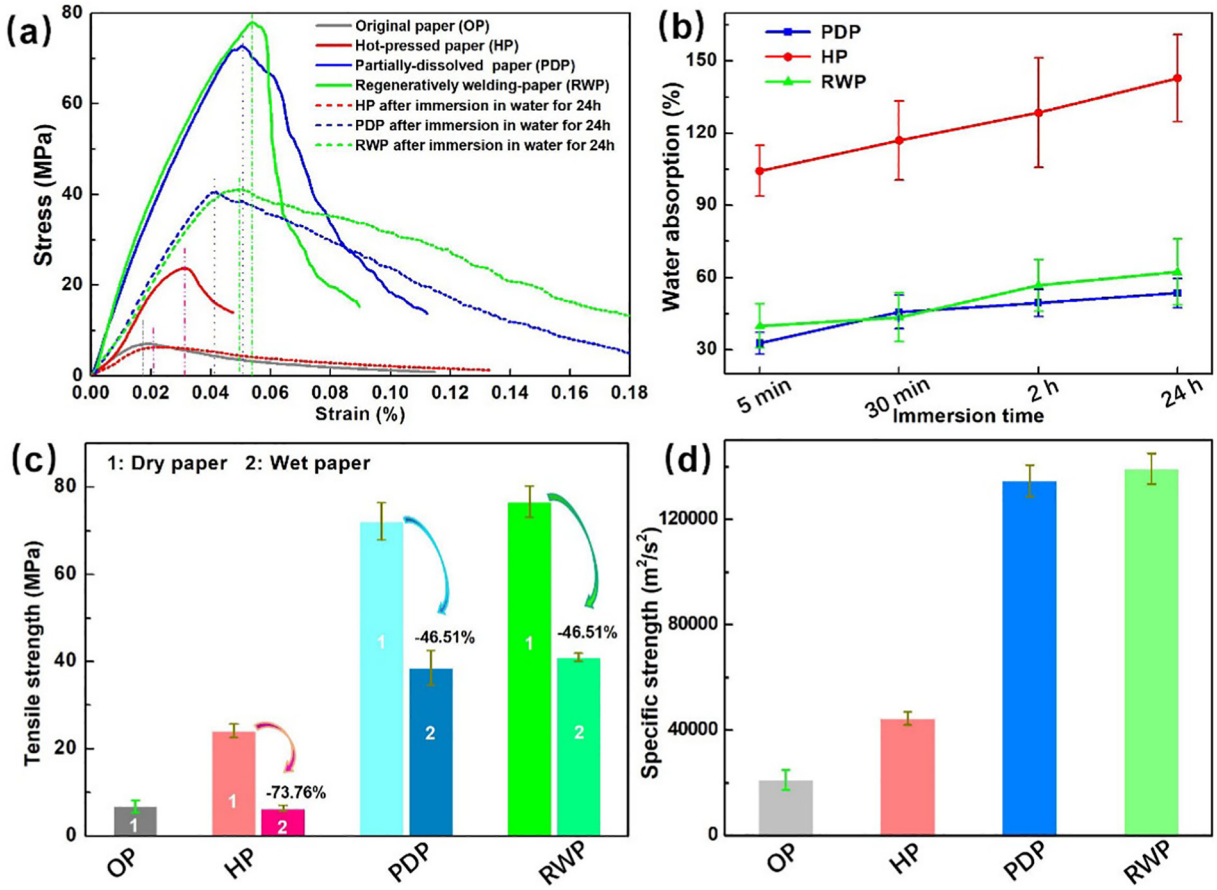

Fig. 6. (a) The stress–strain curves of the aramid paper and (b) the average water absorption of the four papers after the papers were soaked in water for different time periods. (c) The tensile strengths of the four aramid papers and their changes after 24 h of soaking in water, and (d) a comparison of the specific strength of four kinds of aramid paper.

105.5 J/m^2. In sharp contrast, the average ILSS of the PDP and the RWP were 93.2×10^2 and 109.6×10^2 J/m^2. The average ILSS of the RWP increased by 14.6 and 9.4 times, respectively, when compared with the average ILSS of the OP and HP. As shown in Fig. 6a, RWP exhibited the largest elongation at break among the papers, followed by PDP, HP, and OP. The elongation at break of the wet paper was reduced but was consistent with the aforementioned trends because the uniformity and the compactness of the interwoven fibers and their strong bonding force considerably contributed to the folding resistance, the ILSS strength, and the elongation at break of the papers. Notably, the strength indices of the RWP were better than those of the PDP, which can be attributed to the fact that the distribution of MAFs in the paper is not considerably uniform because of the influence of the papermaking process, resulting in an uneven distribution of the meta-aramid regenerated after partial dissolution in the paper. However, no similar problem was encountered in the case in which the meta-aramid solution was directly added dropwise to the paper comprising only the PACFs and the PAPFs for enhancing the regeneration. The average specific strengths of the OP, HP, PDP, and RWP were 21.2×10^3, 44.5×10^3, 134.7×10^3, and 139.2×103 m^2/s^2, respectively. The specific strength of the RWP increased by 5.6 and 2.1 times, respectively, when compared with those of the OP and HP, favoring its potential application as a lightweight high-strength material.

Fig. 8a shows the thermogravimetric analysis (TGA) curves for the PACFs, PAPFs, MAFs, HP, PDP, and RWP. The MAFs began to decompose when the temperature reached 435 °C, whereas the PACFs began to decompose when the temperature reached 540 °C, indicating that both types of fibers exhibited good thermal

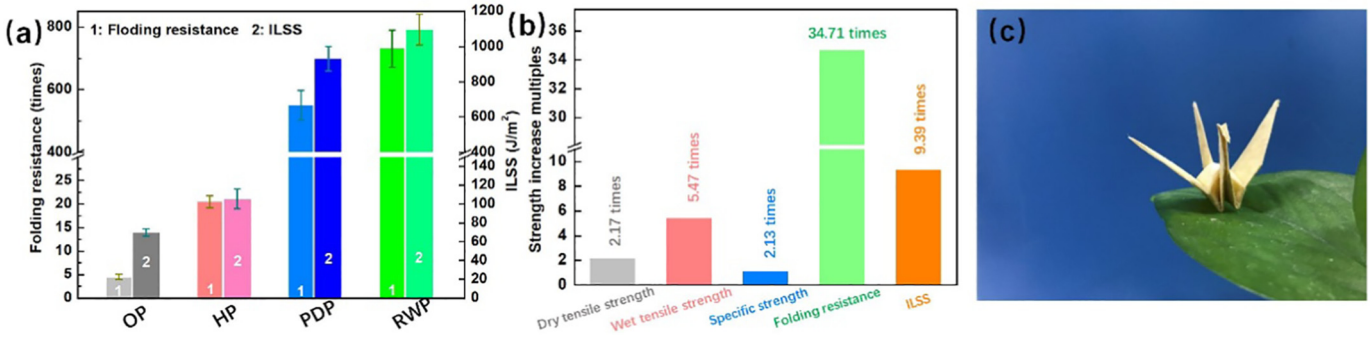

Fig. 7. (a) The average folding resistance and ILSS for four kinds of aramid paper and (b) the multiple by which the mechanical properties of RWP increase when compared to those of HP. (c) A paper crane folded from RWP.

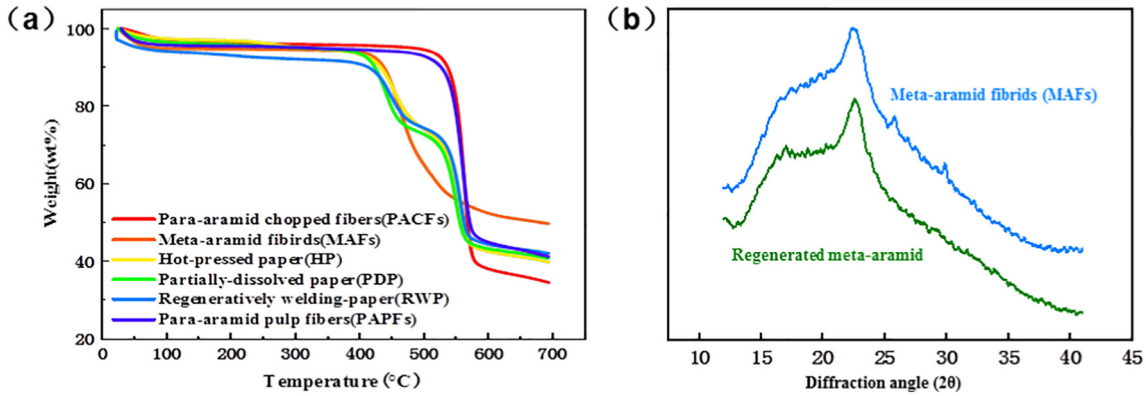

Fig. 8. (a) The TGA curves of the PACFs, PAPFs, MAFs, HP, PDP, and RWP. (b) XRD patterns of the MAFs and regenerated meta-aramid.

stability. Two distinct weightlessness stages were observed in the curves of the OP, PDP, and RWP papers, the first apparent weightlessness occurs at 435 °C and second at 540 °C, which correspond to the decomposition of the para- and meta-aramid in the papers. Notably, the TGA curves of the OP, PDP, and RWP were almost identical, denoting that the thermal properties of the MAFs before dissolution and those of the regenerated meta-aramid were highly consistent. Fig. 8b shows the XRD analysis results for the MAFs before dissolution and the regenerated meta-aramid. The two patterns are observed to be basically the same. Given their similar thermal properties, we deduce that the crystallinity and chemical composition of the MAFs before and after dissolution and regeneration remain unchanged.

4. Conclusion

In summary, the para-aramid/meta-aramid composite papers, exhibiting amazing mechanical strengths, were obtained by two enhancement methods, including partially dissolved regeneration welding and all meta-aramid solution regeneratively welding. The analyses of the FT–IR spectra showed that the enhanced papers exhibited considerable hydrogen bond association. An extremely dense and compact paper structure was observed using SEM. In comparison with the OP, the enhanced papers exhibited both excellent water resistance and ultrahigh mechanical energy. Further, the excellent flexibility and the specific strength of the enhanced papers improve their application for preparing new lightweight high-strength materials such as high-performance aramid paper honeycomb. In addition, the regenerated meta-aramid still retains similar thermal properties to those before dissolution, providing the enhanced papers with a considerably good thermal stability. This study provides a viable alternative method for manufacturing high-performance aramid paper-based materials.

CRediT authorship contribution statement

Ke Xu: Data curation, Formal analysis, Writing - original draft, Writing - review & editing. **Yanghao Ou:** Data curation.**Yinghui Li:** Formal analysis.**Lingfeng Su:**Methodology. **Yang Li:** Formal analysis. **Detao Liu:** Conceptualization, Methodology, Supervision, Writing - original draft, Writing - review & editing.

Declaration of competing interest

The authors declare that they have no known competing financial interests or personal relationships that could have appeared to influence the work reported in this paper.

Acknowledgments

This work was financially supported by the Guangzhou Science and Technology Plan Project (Grant No. 201704030066), Science and Technology Planning Project of Guangdong Province, China (Grant No. 2016B090918074. Guangdong Province Science Foundation for Cultivating National Engineering Research Center for Efficient Utilization of Plant Fibers (2017B090903003).

References

[1] L. Jing, X. Wang, L. Liu, Y. Kim, N.A. Kotov, High strength conductive composites with plasmonic nanoparticles aligned on aramid nanofibers, Adv. Funct. Mater. 26 (46) (2016) 8435–8445.
[2] S.O. Tung, S.L. Fisher, N.A. Kotov, L.T. Thompson, Nanoporous aramid nanofibre separators for nonaqueous redox flow batteries, Nat. Commun. 9 (1) (2018) 4193.
[3] Z. Jiaqi, C. Wenxin, Y. Mingli, H. Ying, H. Jiecai, Y. Ming, Strong and stiff aramid nanofiber/carbon nanotube nanocomposites, ACS Nano 9 (3) (2015) 2489–2501.
[4] S.O. Tung, S. Ho, M. Yang, R. Zhang, N.A. Kotov, A dendrite-suppressing composite ion conductor from aramid nanofibres, Nat. Commun. 6 (2015) 6152.
[5] Z.Y. Shi, P. Cui, X. Li, A review on research progress of machining technologies of carbon fiber-reinforced polymer and aramid fiber-reinforced polymer, Proc. Inst. Mech. Eng. C J. Mech. Eng. Sci. 233 (13) (2019) 4508–4520.
[6] C. Zheng, L. Zhang, J. Chan, D. Yu, C. Meng, L. Luo, X. Liu, Aramid fiber with excellent interfacial properties suitable for resin composite in a wide polarity range, Chem. Eng. J. 347 (2018) 483–492.
[7] J.M. García, F.C. García, F. Serna, J.L.D.L. Peña, High-performance aromatic polyamides, Prog. Polym. Sci. 35 (5) (2010) 623–686.
[8] N. Dadkar, B.S. Tomar, B.K. Satapathy, Evaluation of flyash-filled and aramid fibre reinforced hybrid polymer matrix composites (PMC) for friction braking applications, Mater Design 30 (10) (2009) 4369–4376.
[9] B.A. Patterson, M.H. Malakooti, J. Lin, A. Okorom, H.A. Sodano, Aramid nanofibers for multiscale fiber reinforcement of polymer composites, Compos. Sci. Technol. 161 (2018) 92–99.
[10] M. Lin, Y. Li, K. Xu, Y. Ou, L. Su, X. Feng, J. Li, H. Qi, D. Liu, Thermally conductive nanostructured aramid dielectric composite films with boron nitride nanosheets, Compos. Sci. Technol. 175 (2019) 85–91.
[11] X. Chen, W. Wang, S. Li, C. Jiao, Fire safety improvement of para-aramid fiber in thermoplastic polyurethane elastomer, J. Hazard. Mater. 324 (Pt B) (2017) 789–796324.
[12] Y.J. Wu, J.C. Seferis, V. Lorentz, Evaluations of an aramid fiber in nonwoven processes for honeycomb applications, J. Appl. Polym. Sci. 86 (5) (2002) 1149–1156.
[13] J.M. García, F.C. García, F. Serna, J.L.D.L. Peña, High-performance aromatic polyamides, Prog. Polym. Sci. 35 (5) (2010) 623–686.
[14] A. Russo, B.Y. Ahn, J.J. Adams, E.B. Duoss, J.T. Bernhard, J.A. Lewis, Pen-on-paper flexible electronics, Adv. Mater. 23 (30) (2011) 3426–3430.
[15] H. Kim, S. Lee, H. Kim, Electrical heating performance of electro-conductive para-aramid knit manufactured by dip-coating in a graphene/waterborne polyurethane composite, Sci Rep-UK 9 (1) (2019) 1511.
[16] M. Li, Z. Li, J. Wang, C. Wang, S. Lu, Screen printed silver patterns on functionalised aramid fabric, Fibers & Polymers 18 (10) (2017) 1975–1980.
[17] J.P. Nunes, J.F. Silva, 5-Sandwiched composites in aerospace engineering, Advanced Composite Materials for Aerospace Engineering (2016) 129–174.
[18] P. Przybysz, M. Dubowik, M.A. Kucner, K. Przybysz, B.K. Przybysz, Contribution of hydrogen bonds to paper strength properties, PLoS One 11 (5) (2016), e0155809.
[19] S. Rina, Y. Yan, W. Zhenhai, Z. Liqun, W. Wencai, T. Ming, Surface modification of aramid fibers by bio-inspired poly(dopamine) and epoxy functionalized silane grafting, ACS Appl Mater Inter 6 (23) (2014) 21730–21738.

[20] X. Chen, W. Wang, C. Jiao, A recycled environmental friendly flame retardant by modifying Para-aramid fiber with phosphorus acid for thermoplastic polyurethane elastomer, J. Hazard. Mater. 331 (2017) 257–264.
[21] L. Wang, Y. Shi, R. Sa, N. Ning, W. Wang, M. Tian, L. Zhang, Surface modification of aramid fibers by catechol/polyamine co-deposition followed Silane grafting for the enhanced interfacial adhesion to rubber matrix, Ind. Eng. Chem. Res. 55 (49) (2016) 12547–12556.
[22] Y. Ou, M. Lin, L. Su, X. Feng, M. Wang, J. Li, D. Liu, H. Qi, Highly mechanical nanostructured aramid-composites with gradient structures, Compos. A: Appl. Sci. Manuf. 118 (2019) 250–258.
[23] W. Lei, Y. Shi, S. Chen, W. Wang, T. Ming, N. Ning, L. Zhang, Highly efficient mussel-like inspired modification of aramid fibers by UV-accelerated catechol/polyamine deposition followed chemical grafting for high-performance polymer composites, Chem. Eng. J. 314 (2017) 583–593.
[24] J. Zhu, Y. Li, Q. Guan, G. Liang, A. Gu, A novel strategy of fabricating high performance UV-resistant aramid fibers with simultaneously improved surface activity, thermal and mechanical properties through building polydopamine and graphene oxide bi-layer coatings, Chem. Eng. J. 310 (2017) 134–147.
[25] M. Kanerva, S. Korkiakoski, K. Lahtonen, J. Jokinen, E. Sarlin, S. Palola, A. Iyer, P. Laurikainen, X.W. Liu, M. Raappana, DLC-treated aramid-fibre composites: tailoring nanoscale-coating for macroscale performance, Compos. Sci. Technol. 171 (2019) 62–69.
[26] J. Nasser, J. Lin, K. Steinke, H.A. Sodano, Enhanced interfacial strength of aramid fiber reinforced composites through adsorbed aramid nanofiber coatings, Compos. Sci. Technol. 174 (2019) 125–133.
[27] C.X. Wang, M. Du, J.C. Lv, Q.Q. Zhou, Y. Ren, G.L. Liu, D.W. Gao, L.M. Jin, Surface modification of aramid fiber by plasma induced vapor phase graft polymerization of acrylic acid. I. Influence of plasma conditions, Appl. Surf. Sci. 349 (2015) 333–342.
[28] Y. Hao, W. Wang, D. Yang, X. Zhou, Z. Zhao, Z. Li, S. Wang, F. Jing, Hydrophilicity modification of aramid fiber using a linear shape plasma excited by nanosecond pulse, Surf Coat Tech 344 (2018) 614–620.
[29] L. Xing, L. Li, Y. Huang, D. Jiang, J. Bo, J. He, Enhanced interfacial properties of domestic aramid fiber-12 via high energy gamma ray irradiation, Composites Part B 69 (2015) 50–57.
[30] L. Xing, L. Li, X. Fei, Y. Huang, Mutual irradiation grafting on indigenous aramid fiber-3 in diethanolamine and epichlorohydrin and its effect on interfacially reinforced epoxy composite, Appl. Surf. Sci. 375 (2016) 65–73.
[31] C. Zheng, B. Li, J. Huang, C. Teng, L. Yang, W. Xu, X. Liu, Covalent modification of aramid fibers' surface via direct fluorination to enhance composite interfacial properties, Mater Design 106 (2016) 216–225.
[32] Y. Ou, J. Chen, P. Lu, F. Cheng, M. Lin, L. Su, J. Li, D. Liu, Rapid ILs-polishing processes toward flexible nanostructured paper with dually high transparency and haze, Sci Rep-UK 7 (1) (2017) 6943.
[33] P. Lu, F. Cheng, Y. Ou, M. Lin, L. Su, S. Chen, X. Yao, D. Liu, Rapid fabrication of transparent film directly from wood fibers with microwave-assisted ionic liquids technology, Carbohyd Polym 174 (2017) 330–336.
[34] H. Yousefi, M. Mashkour, R. Yousefi, Direct solvent nanowelding of cellulose fibers to make all-cellulose nanocomposite, Cellulose 22 (2) (2015) 1189–1200.
[35] P. Lu, F. Cheng, Y. Ou, M. Lin, L. Su, S. Chen, X. Yao, D. Liu, A flexible and transparent thin film heater based on a carbon fiber/heat-resistant cellulose composite, Compos. Sci. Technol. 153 (2017) 1–6.
[36] H.L. Lin, Y.C. Chen, C.C. Li, C.P. Cheng, T.L. Yu, Preparation of PBI/PTFE composite membranes from PBI in *N,N′*-dimethyl acetamide solutions with various concentrations of LiCl, J. Power Sources 181 (2) (2008) 228–236.
[37] D. Ahn, J. Lee, C. Kang, Physico-chemical properties of new composite polymer for heat resistance with thin-film form through the blending of m -aramid and polyurethane (PU), Polymer 138 (2018) 17–23.
[38] C. Junho, K. Seung-Yeop, Solvent-assisted heat treatment for enhanced chemical stability and mechanical strength of meta -aramid nanofibers, European Polymer Journall 107 (2018) 46–53.
[39] L. Mazzocchetti, T. Benelli, E. Maccaferri, S. Merighi, J. Belcari, A. Zucchelli, L. Giorgini, Poly-m-aramid electrospun nanofibrous mats as high-performance flame retardants for carbon fiber reinforced composites, Composites Part B Engineering 145 (2018) 252–260.
[40] S.Y. Ryu, J.W. Chung, S.Y. Kwak, Amphiphobic meta -aramid nanofiber mat with improved chemical stability and mechanical properties, Eur. Polym. J. 91 (2017) 111–120.
[41] Z. Sufeng, L. Penghui, L. Yuan, L. Dan, L. Ye, Effect of hot pressing temperature on inter-binding feature between Para-aramid fiber and meta-aramid fibrids in composite paper, Acta Materiae Compositae Sinica 35 (4) (2017) 1003–1008.
[42] B. Yang, M.Y. Zhang, L.I. Tao, S.F. Zhang, Analysis on the Structure of Hydrogen Bond of Aramid Paper Fibers by FT-IR, Paper & Paper Making, 12, 2011 24.
[43] S.F. Zhang, Z.X. Sun, Q. Wang, J. Sun, Adhesion properties of meta-aramid composite paper in the hot calendaring process, Paper & Paper Making (2013) 3.
[44] Z.X. Sun, S.F. Zhang, W.W. Dou, Study on interfacial performance of aramid composite paper, Paper Science & Technology (2015) 2.
[45] Y. Bin, Z. Meiyun, L. Zhaoqing, L. Jingjing, S. Shunxi, T. Jiaojun, Z. Qiuyu, Toward improved performances of Para-aramid (PPTA) paper-based nanomaterials via aramid nanofibers(ANFs) and ANFs-film, Compos. Part B 154 (2018) 166–174.